Optical Fiber Technology 89 (2025) 104045

Contents lists available at ScienceDirect

Optical Fiber Technology

journal homepage: www.elsevier.com/locate/yofte

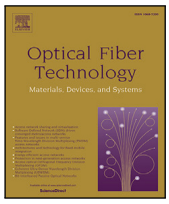

Relay aided UWOC-SMF-FSO based hybrid link for underwater wireless optical sensor network

Jawad Mirza [a,b], Ahmad Atieh [c], Benish Kanwal [d], Salman Ghafoor [e], Ahmad Almogren [f], Firdos Kanwal [d], Imran Aziz [g,d,*]

[a] SEECS Photonics Research Group, Islamabad, Pakistan
[b] Electrical Engineering Department, HITEC University Taxila, Pakistan
[c] Optiwave Systems Inc., Ottawa, Ontario, Canada
[d] Electrical Engineering Department, Mirpur University of Science and Technology (MUST), Mirpur (AJK), Pakistan
[e] School of Electrical Engineering and Computer Science (SEECS), National University of Sciences and Technology (NUST), H-12, Islamabad, Pakistan
[f] Department of Computer Science, College of Computer and Information Sciences, King Saud University, Riyadh, Saudi Arabia
[g] Department of Physics and Astronomy, Uppsala University, Uppsala, Sweden

ARTICLE INFO

Keywords:
Internet of underwater things
Remotely operated underwater vehicle
Underwater wireless optical communication
Free space optics
Wavelength translation
Intensity modulation- direct detection
Gamma–gamma channel model
Line of sight communication
Optical relay

ABSTRACT

The Internet of Underwater Things (IoUTs) connects underwater devices to communicate, sense surroundings, and transmit data. Acoustic communication faces bandwidth limitations, making underwater wireless optical communication-free space optics (UWOC-FSO) hybrid systems a promising alternative. However, maintaining sufficient power budget and signal-to-noise ratio (SNR) is a challenging task, making wavelength translation (WT) from visible to infrared (IR) at the water-fiber-air interface crucial for reliable signal transmission. In this paper, we propose an underwater wireless optical communication-single mode fiber-free space optics (UWOC-SMF-FSO) hybrid link based on a photo-detection, remodulate, and forwarding (PRF) relay and intensity modulation-direct detection (IM/DD) scheme for 8 × 1-Gb/s underwater optical wireless sensor network (UWOSN). The PRF relay is installed at a remotely operated underwater vehicle (ROV) to perform WT from visible range to IR. The performance of the sensors is analyzed for different water bodies and weather conditions of underwater and free space optics channels, respectively using metrics of Bit-error rate (BER) and Quality factor (Q-factor) employing Gamma–Gamma channel model. The simulation results show that forward-error correction (FEC) target BER of 10^{-4} for sensors is achieved under different water bodies and weather conditions. The results obtained from this study show that the proposed UWOC-SMF-FSO hybrid link is flexible, resilient to adverse channel effects, and can be a potential candidate for implementation of high-speed long-distance future IoUTs.

1. Introduction

Major portion of the earth's surface area is covered by water which accounts for approximately 72% or 509 million km^2 [1,2]. Considering the recent development of the world's economy, land resources are rapidly depleting and soon will become insufficient to cater the growing needs of mankind [3]. The oceans are rich in natural resources and will play an important role for meeting the needs of human population [3]. Consequently, the scientists have become more and more interested in exploring the underwater world, leading to technological advancements towards creating Internet of Underwater Things (IoUTs) [1,2]. IoUTs refer to the network of interconnected devices and sensors that communicate with each other and the surface control centers in various underwater applications [1]. This concept extends the Internet of Things (IoTs) specifically designed for underwater environments to explore the oceans for various tasks such as underwater surveys, discovering natural resources, detecting early signs of tsunamis, monitoring animal health, obtaining real-time aquatic information, and conducting archaeological expeditions [3].

Underwater wireless sensor networks (UWSNs) play a key role in realizing the IoUT. UWSNs are the backbone of the IoUTs, providing the necessary infrastructure for underwater communication and data exchange between the IoUTs and offshore data centers [4]. However, traditional UWSNs based on acoustic and radio frequency (RF) communications have various limitations. For example, the transmission distance of RF-based UWSNs is limited by strong attenuation in water [3]. Meanwhile, acoustic communication, which is widely

* Corresponding author.
E-mail address: imran.aziz@physics.uu.se (I. Aziz).

https://doi.org/10.1016/j.yofte.2024.104045
Received 21 August 2024; Received in revised form 23 October 2024; Accepted 9 November 2024
Available online 21 November 2024

used in UWSNs, can achieve long-distance transmission, but it suffers from low data rates and long propagation delay [3]. Wireless optical communications (WOC) has attracted a lot of attention in the past two decades. Terrestrial WOC is also called free space optics (FSO) communication has several advantages over current RF and microwave communication systems, including un-licensed spectrum utilization, extremely large bandwidth, long distance, high bit rates, speedy deployment, low maintenance cost, security from eavesdropping, and immunity to electromagnetic interference (EMI) [5]. FSO systems support high data rates comparable to fiber optic communication ranging from Gb/s to Tb/s but at a fraction of its deployment and maintenance costs [6]. FSO system is ideal for many applications, such as inter-building communication, military applications, metro network extension, enterprise connectivity, fiber back-up, mobile backhaul links, last-mile access, free-space laser communications including airborne, space borne, and deep space missions [7]. Similarly, WOC in aquatic domain is called underwater wireless optical communication (UWOC) which has attracted much attention recently due to its high data rates, low latency, and transmission range up to hundreds of meters [8]. UWOC plays a key role in pollution monitoring, environmental monitoring, marine exploration, live video streaming, marine archaeology, image processing, oceanography, port security, petroleum pipeline maintenance, disaster response, tactical surveillance, and underwater optical wireless sensor networks [7]. UWOC has become an attractive alternative to traditional RF and acoustic communications owing to aforementioned benefits. Therefore, UWOC-FSO convergent system is a promising solution to resolve the connectivity related issues in UWSNs [9]. However, optical signals transmitted over FSO and UWOC channels can be affected by various detrimental factors, including atmospheric attenuation, intensity scintillation, water absorption, geometric losses etc. [2,6].

Hybrid optical interconnects combine different optical communication technologies to create a single integrated system that leverages the strengths of each technology. These interconnects aim to overcome the limitations of the individual technologies and improve performance, flexibility, and reliability. Examples of hybrid optical links are (I) FSO-RF, (II) UWOC-Acoustic, (III) Fiber-FSO, (IV) UWOC-Fiber, (V) FSO-UWOC, and (VI) UWOC-Fiber-FSO [10]. UWOC-SMF-FSO based hybrid links combine three technologies to enable reliable high-speed data transmission over long distances for a variety of applications including UWSNs. The benefits of this particular type of hybrid link include improved communication reliability and longer transmission distances. UWOC enables high-speed data transmission underwater, while SMF enables stable data transmission with low loss over long distances in terrestrial networks. FSO complements the system by enabling wireless communication, bridging gaps where fiber is not practical. This hybrid approach improves network stability, supports high data rates, and overcomes challenges posed by underwater and terrestrial environments. For UWOC-SMF-FSO based hybrid links, wavelength conversion from the visible spectrum to the infrared spectrum is required to improve the power budget and SNR to extend the overall range of the hybrid link.

1.1. Literature survey

Hybrid optical links are widely discussed in literature such as UWOC-SMF hybrid link for monitoring the underwater temperature and pressure for sea divers [2], optical-acoustic hybrid link for underwater wireless optical sensor networks based power control aided routing protocol [4], multi-hop convergent FSO-UWOC link for establishing a reliable communication link between the islands [7], FSO-UWOC convergent link based on five-wavelength polarization multiplexing [9], visible light communication (VLC) and optical camera communication (OCC) based hybrid system for indoor IoTs [10], dual-hop FSO-UWOC hybrid link for air to ocean transmission [11], VLC-RF hybrid link based on cooperative relaying [12], FSO-VLC hybrid link based on four level pulse amplitude modulation (PAM4) and non-orthogonal multiple access (NOMA) [13], wavelength division multiplexing (WDM) UWOC-FSO hybrid link based on PAM-4 [14], high altitude platform station (HAPS) integrated FSO-RF-UWOC hybrid link based on decode and forward (DF) relay [15], unmanned aerial vehicle (UAV) based dual-hop FSO-UOWC hybrid link [16], and FSO-SMF hybrid link based on WDM, polarization division multiplexing (PDM), and quadrature modulation (QAM) [17]. To further elaborate on the literature review, the major achievements of previously published studies are presented in Table 1 and finally compared with the proposed work. From detailed literature review, it is evident that UWOC-SMF-FSO based hybrid link employing PRF relay for WT from visible range to IR is a novel solution for the implementation of the UWOSNs that has not yet been studied. Therefore, to the best of our knowledge, the proposed work is introduced for the first time in the literature. We report an UWOC–SMF–FSO hybrid link based on WT from visible range to IR for 8 × 1-Gb/s UWOSN. The WT is performed using a single PRF relay installed at ROV. Transmission of sensors' data at an aggregate rate of 8 Gb/s encoded using non-return to zero on-off keying (NRZ-OOK) modulation format over UWOC-SMF-FSO based hybrid link has been achieved. Performance of the sensors is analyzed through simulation results considering different water bodies and weather conditions of UWOC and FSO channels, respectively using Gamma–Gamma channel model for FEC target BER of 10^{-4}. Considering the above discussion, the major achievements of this study are as follows:

- Hybrid optical link based on the seamless integration of UWOC, SMF, and FSO is proposed for 8 × 1-Gb/s UWOSN employing a PRF relay for WT from visible range to IR.
- Transmission of sensors' data at a combined rate of 8 Gb/s of sensors encoded using NRZ-OOK modulation format over UWOC-SMF-FSO based hybrid link has been achieved.
- Performance of sensors is analyzed considering different water bodies and weather conditions of UWOC and FSO channels, respectively using Gamma–Gamma channel model.

We have implemented the proposed work using "OptiSystem 21" simulation software developed by Optiwave Inc [18,19]. The paper is structured as follows. Section 2 discusses the application scenario of the proposed work, Section 3 presents the system and channel models, Section 4 describes the proposed setup, Section 5 discusses the results, and finally Section 6 concludes the paper.

2. Application scenario of the proposed link

An application scenario of the proposed UWOC-SMF-FSO based hybrid link employing a PRF relay for UWOSN and IoUTs has been shown in Fig. 1. It may be observed that underwater sensors, AUVs, surface and cruise ships, relays, buoys, satellites, and ground elements (e.g. seashore base stations, control centers, and data centers) constitute the components of UWOSN and IoUTs. The sensors first gather important ocean data, then transmit it to the PRF relay enabling the UWOC-SMF-FSO based high-speed hybrid link towards ground based control center where the data is recovered and processed by experts for further analysis.

3. System and channel model

The PRF relay is connected between the sensors and the standard single-mode fiber (SSMF) connecting the relay with surface ship. Therefore, a terrestrial FSO link is established between the surface ship and ground based control center.

Table 1
Published related work and comparison of their important results with the proposed study.

Study	Link	WT	Total range	Total data rate	No. of sensors	Modulation
[2]	UWOC–SMF	✘	0.85 km	–	2	IM
[4]	Acoustic–UWOC	✘	0.4 km	–	5	OOK
[7]	FSO–UWOC	✘	2.02 km	–	–	DPSK
[9]	UWOC–FSO	✘	0.215 km	500 Gb/s	10	PAM4
[10]	VLC–OCC	✘	0.004 km	100 Mb/s	1	OOK
[11]	FSO–UWOC	✘	0.035 km	1 Gb/s	1	BPSK
[12]	VLC–RF–FSO	✘	0.81 km	–	1	OOK-BPSK
[13]	VLC-FSO	✘	10.002 km	10 Gb/s	2	PAM4
[14]	FSO–UWOC	✘	0.505 km	100 Gb/s	2	PAM4
[17]	FSO–SMF	✘	53.5 km	448 Gb/s	4	QAM
Proposed	UWOC–SMF–FSO	✔	5.04 km	8 Gb/s	8	NRZ-OOK

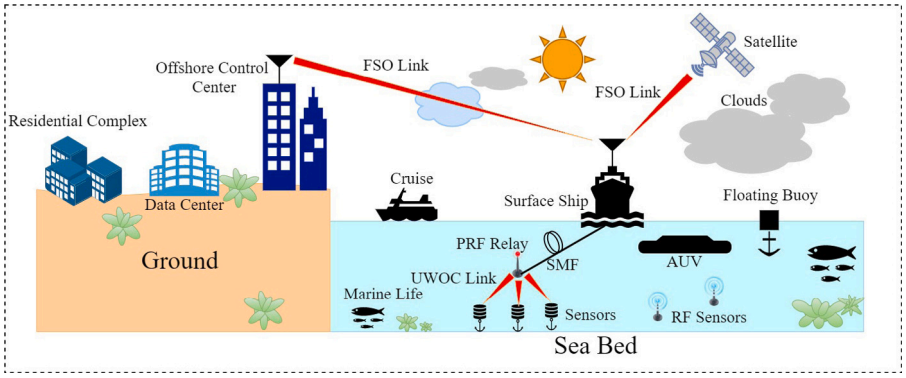

Fig. 1. Illustration of application scenario of the proposed link in UWOSN and IoUTs, **UWOC**: Underwater wireless optical communication link, **PRF**: Photodetect, remodulate, and forward relay, **SMF**: Standard single-mode fiber, **RF**: Radio frequency sensor, **AUV**: Autonomous underwater vehicle, and **FSO**: Free space optics link.

Table 2
Absorption, scattering, and extinction coefficients for different water bodies specified at wavelength of 532 nm.

Water body	$a(\lambda)$ (m^{-1})	$b(\lambda)$ (m^{-1})	$c(\lambda)$ (m^{-1})
Pure sea	0.0405	0.0025	0.043
Clean ocean	0.114	0.037	0.151
Coastal ocean	0.179	0.219	0.398
Harbor I	0.187	0.913	1.1
Harbor II	0.366	1.824	2.19

3.1. UWOC system and channel model

The total received power for line-of-sight UWOC system can be expressed as [2,20].

$$P_r = P_t \eta_t \eta_r \exp\left[-c(\lambda)\frac{d}{\cos\theta}\right] \frac{A_r \cos\theta}{2\pi d^2(1-\cos\theta_o)} \quad (1)$$

In above equation, P_t is the average transmitted power, η_t is the efficiency of the transmitter, η_r is the efficiency of the receiver, d is the perpendicular distance between the transmitter and the receiver planes, θ is the angle between the perpendicular to the receiver plane and the transmitter–receiver trajectory, A_r is the receiver aperture area, and θ_o is the beam divergence which characterizes the geometric and pointing losses. The total signal attenuation of an optical signal propagating through a body of water is given by [2,20].

$$c(\lambda) = a(\lambda) + b(\lambda) \quad (2)$$

where, $c(\lambda)$ is the extinction coefficient, $a(\lambda)$ is the absorption coefficient, and $b(\lambda)$ is the scattering coefficient. It is clearly evident from Eq. (2) that the values of absorption and scattering coefficients rely upon the optical characteristics of the water body and operating wavelength. In this study, different water bodies were considered, whose extinction, absorption, and scattering coefficients are given in Table 2.

3.2. FSO system and channel model

Similarly, the total received optical power for line-of-sight FSO system can be expressed as [13].

$$P_r = P_t \left[\frac{\lambda}{4\pi d}\right]^2 G_t G_r \eta_t \eta_r \times \frac{1}{L} \quad (3)$$

where, P_t is the transmitted optical power into free space, λ is the operating wavelength, d is the distance between the transmitter and receiver telescopes, and G_t, is the transmitter's gain, G_r is the receiver's gain, η_t is the transmitter's efficiency, η_r is the receiver's efficiency, and L are total system losses which includes alignment losses, connector losses, atmospheric losses due to absorption etc. The optical properties including refractive index of the FSO channel frequently change caused by variations in temperature, humidity, and pressure of the air [6,13]. The random variation in intensity of the received signal due to alteration of air refractive index is called intensity scintillation or atmospheric turbulence [6,13]. The random variation in received signal's intensity is often modeled employing the Gamma–Gamma distribution [6,13]. This channel model is a feasible model to estimate the turbulence-induced fading in FSO systems because it takes into account both small- and large-scale fading edies [21]. The Gamma–Gamma model renders a more precise estimation of turbulence in FSO systems compared to other channel models [13]. The probability density function (pdf) of the received signal intensity using Gamma–Gamma channel model is given by the following equation [21].

$$\rho(I) = \frac{2(\alpha\beta)^{\frac{\alpha+\beta}{2}}}{\Gamma(\alpha)\Gamma(\beta)} I^{(\alpha+\beta)/2-1} K_{\alpha-\beta}\left(2\sqrt{\alpha\beta I}\right) \quad (4)$$

where $K_{\alpha-\beta}$ and $\Gamma(\cdot)$ represent the modified Bessel and Gamma functions, respectively [6,13]. The Gamma function is defined by the following equation [6].

$$\Gamma(d) = \int_0^\infty exp(-t)t^{d-1}dt \quad (5)$$

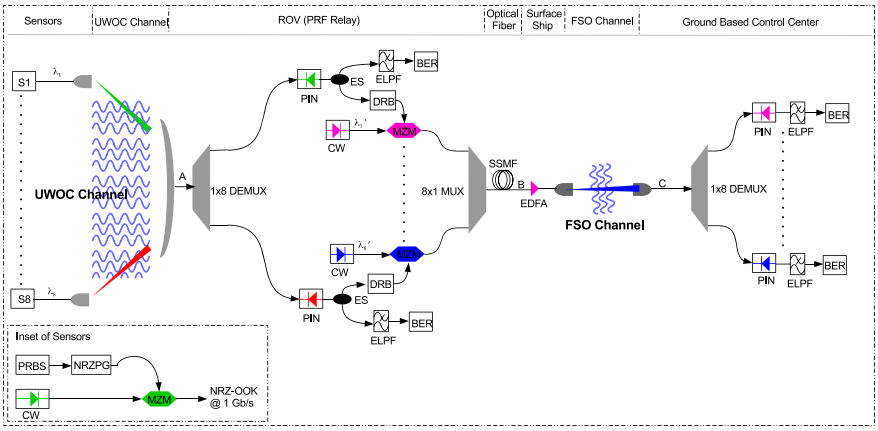

Fig. 2. Schematic of the proposed architecture, **PRBS**: Pseudo random bit sequence generator, **NRZPG**: Non-return to zero pulse generator, **NRZ-OOK**: Non-return to zero on-off keying, **S**: Underwater sensors, **ES**: Electrical splitter, **UWOC**: Underwater wireless optical communication channel, **DEMUX**: Demultiplexer, **PIN**: Positive intrinsic negative photo-detector, **CW**: Continuous wave laser, **DRB**: Data recovery block, **MZM**: Mach-zehnder modulator, **MUX**: Multiplexer, **SSMF**: Standard single-mode fiber, **OA**: Optical amplifier, **FSO**: Free space optics channel, **ELPF**: Electrical lowpass filter, **BER**: Bit-error rate estimator.

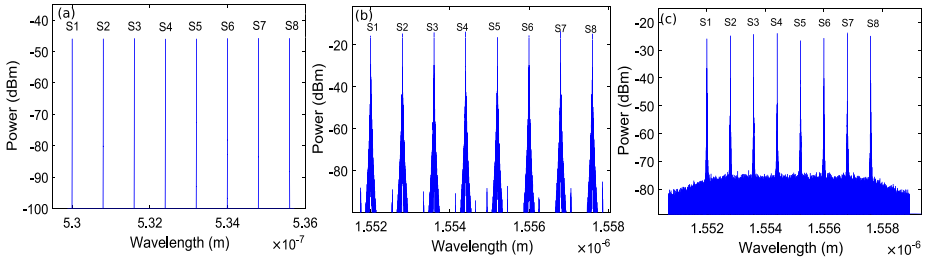

Fig. 3. Spectral plots of combined optical signal at points (a) A (b) B (c) C. These plots are obtained for water body of pure sea, atmospheric attenuation of 2 dB/km, and refractive index structure parameter (C_n^2) of 5×10^{-16} $m^{-2/3}$.

where α and β parameters represent the large and small scale fading edies, respectively and can be expressed by the following equations [6, 21].

$$\alpha = \left[exp\left(\frac{0.49\sigma_R^2}{\left(1 + 1.11\sigma_R^{12/5}\right)^{7/6}} \right) - 1 \right]^{-1} \tag{6}$$

$$\beta = \left[exp\left(\frac{0.51\sigma_R^2}{\left(1 + 0.69\sigma_R^{12/5}\right)^{5/6}} \right) - 1 \right]^{-1} \tag{7}$$

where σ_R^2 is the Rytov variance of received signal's normalized intensity and can be expressed as [6,21].

$$\sigma_R^2 = 1.23 C_n^2 k^{7/6} d^{11/6}, \tag{8}$$

where C_n^2 is known as the refractive index structure parameter that gives a measure of the strength of the atmospheric turbulence, d is the propagation distance and $k = 2\pi/\lambda$ is the optical wave number. We have considered different weather conditions and turbulence regimes in this work characterized by atmospheric attenuation coefficient (α_{atm}) and C_n^2 parameter with values given in Table 3. It is pertinent to mention here that the values of C_n^2 and α_{atm} parameters used in this work are taken similar to multiple studies related to FSO systems [5,6,22,23].

4. Proposed UWOC-SMF-FSO based hybrid link

A comprehensive schematic diagram of the proposed link is shown in Fig. 2. In real world applications, underwater sensors produces analog signals that are digitized using analog to digital converters to create stream of bits [24]. The binary signal is modulated onto a carrier wave and then transmitted over the communication channel. In this work, eight continuous wave (CW) lasers with operating wavelengths

Table 3
Turbulence and attenuation parameters.

Parameters	Turbulence regimes		
	Weak	Moderate	Strong
C_n^2 ($m^{-2/3}$)	5×10^{-17}	5×10^{-13}	5×10^{-10}
α	11.6	4	4.2
β	10.1	1.9	1.4
α_{atm} (dB/km)	5	10	15

of λ_1 = 532 nm, λ_2 = 532.8 nm, λ_3 = 533.6 nm, λ_4 = 534.4 nm, λ_5 = 535.2 nm, λ_6 = 536 nm, λ_7 = 536.8 nm, and λ_8 = 537.6 nm as per 0.8 nm ITU-T wavelength division multiplexing (WDM) spectral grid (ITU-T G.694.1), each has 15 dBm power are used as optical carriers. The generation of underwater sensors' data is simulated using pseudo random bit sequence (PRBS) generators, each at the rate of 1 Gb/s. The binary data of each sensor is then encoded onto a non-return to zero on–off keying (NRZ-OOK) pulse format and used to modulate each optical carrier as shown in inset of Fig. 2. The modulated optical signals of sensors in the visible range are transmitted over line of sight UWOC channel and received by the receiver telescope installed at ROV as shown in Fig. 2. The spectral plot of the combined optical signal at point "A" is shown in Fig. 3(a). The PRF relay is installed at ROV where WT from visible range to IR is achieved. To perform WT, the combined optical signal is demultiplexed using 1 × 8 demultiplexer and each optical signal is then photodetected using positive intrinsic negative (PIN) photo-detector. The electrical signals obtained at the output of each PIN photo-detector are split into two paths. The signals at one of the paths are filtered using an electrical lowpass filter (ELPF) and then passed on to BER estimators for BER measurements. Different water bodies are used in this study to simulate the impact of different types of sea water on the BER performance of the sensors. The signals at other

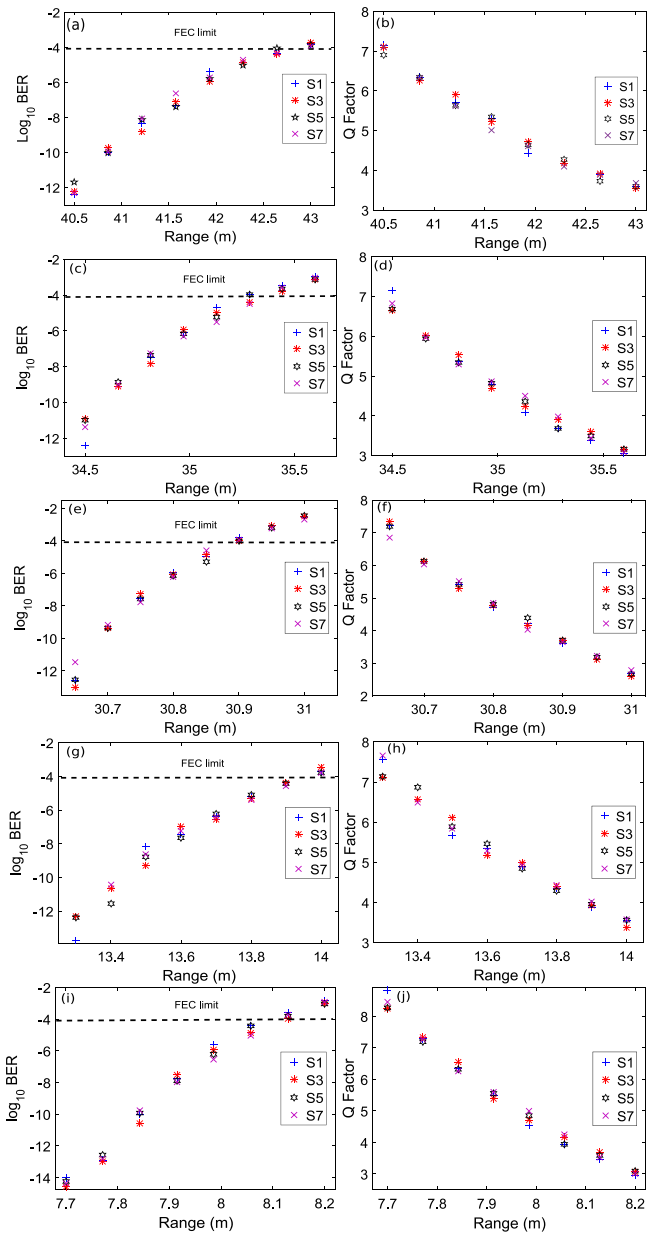

Fig. 4. BER versus (a, c, e, g, and i) UWOC channel range plots for pure sea, clear ocean, coastal ocean, harbor-I, and harbor-II and Q-factor versus (b, d, f, h, and j) UWOC channel range plots for pure sea, clear ocean, coastal ocean, harbor-I, and harbor-II, respectively.

path are applied to data recovery blocks (DRBs) to recover the binary data from the electrical signals while preserving the initial encoding format. The decision instant and the threshold level is automatically calculated by this component. The automatic decision threshold makes the decision based on the average of all samples of the sequence at that level; not the bit, according to the following equation.

$$Average = \frac{\sum_{i=1}^{i=N} A_i}{N} \tag{9}$$

where A_i is amplitude of the ith sample in the total number of samples at that level. The amplitude of the bit sample at the decision instant will be compared to half of the average value. After data recovery, the data are encoded again using NRZ-OOK format and carried over the CW lasers centered at λ'_1 = 1550 nm, λ'_2 = 1550.8 nm, λ'_3 = 1551.6 nm, λ'_4 = 1552.4 nm, λ'_5 = 1553.2 nm, λ'_6 = 1554 nm, λ'_7 = 1554.8 nm, and λ'_8 = 1555.6 nm with 0.8 nm ITU-T WDM

Table 4
Key parameters used in the simulation study.

Parameter	Value
Data rate of each sensor	1 Gb/s
Power of each CW laser in visible range	15 dBm
Power of each CW laser in IR range	0 dBm
Extinction ratio of each MZM	30 dB
Beam divergence	2 mrad
Transmitter and receiver aperture dia	5 cm and 20 cm
Coupling efficiency	90%
Bandwidth of MUX and DEMUX	5 GHz
Length of SSMF	0 and 1 km
Attenuation of SSMF	0.2 dB/km
Dispersion	16.75 ps/nm/km
Gain and NF of EDFA	20 dB and 4 dB
Responsivity of PIN photo-detectors	0.9 A/W
Power density of thermal noise	100×10^{-24} W/Hz
Cut-off frequency of ELPFs	0.75 GHz

spectral grid (ITU-T G.694.1), where each laser has 0 dBm power. The data modulated optical signals in IR range are combined using 8 × 1 multiplexer and transmitted over SSMF towards the surface ship which could be away by ranges over 1 km. The spectral plot of the combined optical signal at point "B" is shown in Fig. 3(b). The combined optical signal at the output of SSMF that is received at the surface ship and amplified using an Erbium-doped fiber amplifier (EDFA), as shown in Fig. 2. The spectral plot of the combined optical signal at point "C" is shown in Fig. 3(c). The amplified signal is then transmitted over line of sight FSO channel using a telescope installed at the surface ship towards ground based control center. It is important to mention here that the scintillation in the FSO channel is modeled using Gamma–Gamma distribution as described above. The combined optical signal is received at the control center using the receiver telescope and demultiplexed using 1 × 8 demultiplexer. Each optical signal is then photo-detected using PIN photo-detectors as shown in Fig. 2. The electrical signals obtained at the output of PIN photo-detectors are again filtered using ELPFs and passed to BER estimators. Different atmospheric attenuation and turbulence values are used in this study to simulate the impact of different types of weather conditions on the BER performance. A comprehensive overview of all the main parameters used in the simulation study is given in Table 4. Simulation parameters as mentioned in Table 4 are chosen as per specifications of commercial components or taken from past published studies [5,6,22,23,25–27].

5. Results and discussion

The following points are assumed in the analysis of the performance of the sensors in this work.

- Sensors are assembled as anchored nodes, close to the sea bed, and at a same distance from ROV.
- Line of sight communication is established between transmitter and receiver telescopes for UWOC and FSO channels.
- The length of SSMF is fixed at 1 km.
- Geometrical loss is considered in UWOC and FSO channels.
- Thermal noise of PDs at ROV is ignored due to low water temperature.
- FEC target BER is set at 10^{-4}.
- Sensor-1,-2,-3, and −4 are randomly selected to discuss the performance while sensor-2 is selected to discuss the eye patterns.

The performance of the sensors is examined at ROV using BER and Q-factor metrics considering various water bodies such as pure sea, clear ocean, coastal ocean, harbor-I, and harbor-II. The BER and Q-factor values are calculated using OptiSystem's built-in statistical method by observing the eye pattern of the received signal at the output of ELPF. For the sake of simplicity, we randomly select only four sensors to

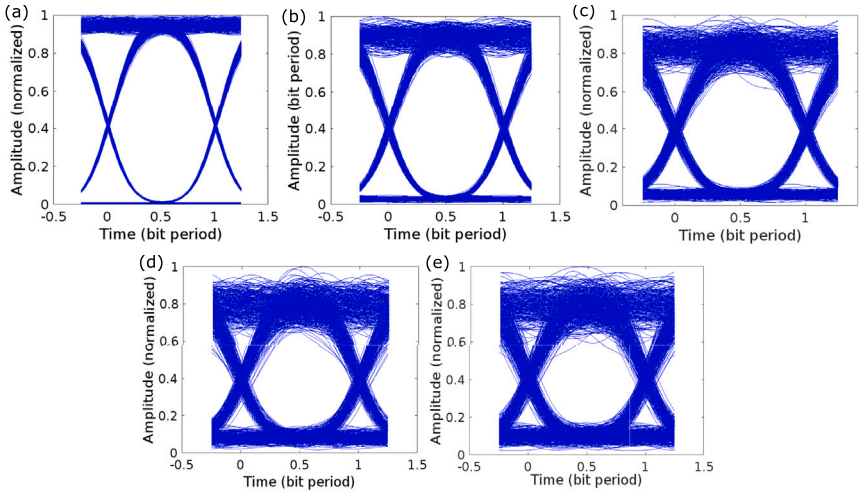

Fig. 5. Normalized eye patterns of sensor-2 for different water bodies (a) Pure sea (b) Clean ocean (c) Coastal ocean (d) Harbor-I and (e) Harbor-II.

discuss their performance here. Fig. 4 shows the plots of BER and Q-factor versus range of UWOC channel for different water bodies. It can be observed from Fig. 4(a), (c), (e), (g), and (i) that maximum range of UWOC channel of 42.7 m, 35.4 m, 30.9 m, 13.9 m, and 8.15 m is achieved at FEC target BER of 10^{-4} for pure sea, clear ocean, coastal ocean, harbor-I, and harbor-II, respectively. It is clear that maximum achievable UWOC channel range at FEC target BER of 10^{-4} decreases for increasing the water attenuation. Similarly, the range of UWOC channel decreases for a particular value of Q-factor on increasing the water attenuation as shown in Fig. 4(b), (d), (f), (h), and (j). To further illustrate the sensors' performance, we obtain the eye patterns of sensor-2 at the output of ELPF for different water bodies as shown in Fig. 5. It is clear that as the value of water attenuation increases, the eye diagram of the received signal deteriorates and becomes narrower.

The end to end performance of the sensors is now analyzed at ground based control center considering different weather and turbulence conditions of FSO channel. It is pertinent to mention here that we used pure sea for UWOC channel. The values of BER and Q factor are calculated using the same method as discussed earlier. By varying the values of the atmospheric attenuation coefficient, different weather conditions such as light haze, heavy haze, dense fog, and heavy rain are simulated. The values of atmospheric attenuation coefficient in the range of 2–21 dB/km are sufficient to cover wide range of weather conditions. Fig. 6 shows the plots of BER and Q-factor versus range of FSO channel for different values of atmospheric attenuation coefficient. It can be observed from Fig. 6(a), (b), and (c) that maximum range of FSO channel of 5.15 km, 1.75 km, and 1.13 km is achieved at FEC target BER of 10^{-4} for atmospheric attenuation coefficient values of 2 dB/km, 11 dB/km, and 21 dB/km, respectively while the value of C_n^2 parameter is 5×10^{-16} $m^{-2/3}$. It is clear that maximum achievable range of FSO channel at FEC target BER of 10^{-4} decreases on increasing the atmospheric attenuation. Similarly, FSO channel range decreases for a particular value of Q-factor on increasing the atmospheric attenuation as shown in Fig. 6(d), (e), and (f). To further illustrate the sensors' performance, we obtain the eye patterns of sensor-2 at the output of ELPF for different values of atmospheric attenuation as shown in Fig. 7. It is evident that as the value of atmospheric attenuation increases, the eye diagram of the received signal becomes degraded and narrower.

Fig. 8 shows the plots of BER and Q-factor versus range of FSO channel for different values of C_n^2 parameter. It can be observed from Fig. 8(a), (b), and (c) that maximum range of FSO channel of 5.15 km, 4.8 km, and 4.7 km is achieved at FEC target BER of 10^{-4} for C_n^2 parameter values of 5×10^{-16} $m^{-2/3}$, 5×10^{-14} $m^{-2/3}$, and 5×10^{-12} $m^{-2/3}$, respectively while the value of atmospheric attenuation is 2 dB/km. It is clear that maximum achievable range of FSO channel at FEC target BER of 10^{-4} decreases on increasing the value of C_n^2 parameter. Similarly, range of FSO channel decreases for a particular value of Q-factor on increasing the value of C_n^2 parameter as shown in Fig. 8(d), (e), and

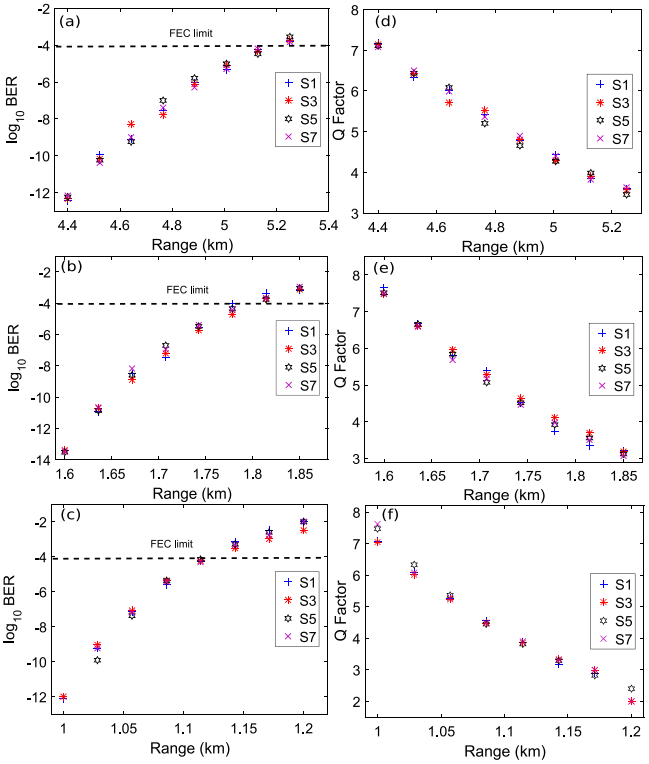

Fig. 6. BER versus (a, b, and c) range of FSO channel plots for atmospheric attenuation values of 2 dB/km, 11 dB/km, and 21 dB/km and Q-factor versus (d, e, and f) range of FSO channel plots for atmospheric attenuation values of 2 dB/km, 11 dB/km, and 21 dB/km, respectively. The value of C_n^2 parameter is 5×10^{-16} $m^{-2/3}$.

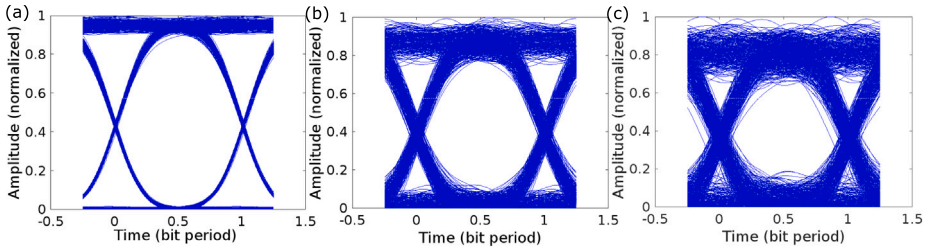

Fig. 7. Normalized eye patterns of sensor-2 for different values of atmospheric attenuation (a) 2 dB/km (b) 11 dB/km and (c) 21 dB/km. The value of C_n^2 parameter is 5×10^{-16} $m^{-2/3}$.

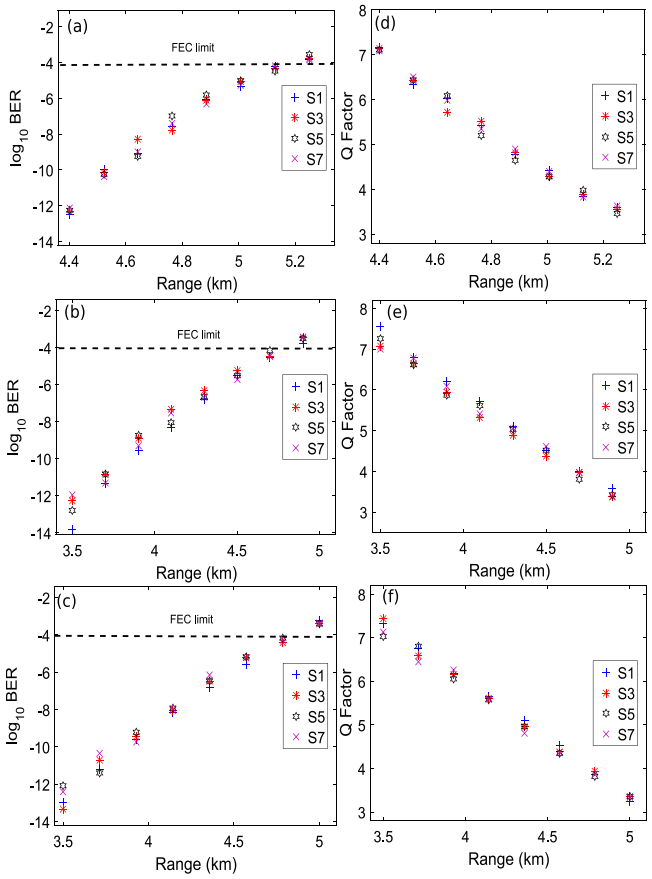

Fig. 8. BER versus (a, b, and c) range of FSO channel plots for C_n^2 parameter values of 5×10^{-16} $m^{-2/3}$, 5×10^{-14} $m^{-2/3}$, and 5×10^{-12} $m^{-2/3}$ and Q-factor versus (d, e, and f) range of FSO channel plots for C_n^2 parameter values of 5×10^{-16} $m^{-2/3}$, 5×10^{-14} $m^{-2/3}$, and 5×10^{-12} $m^{-2/3}$, respectively. The value of atmospheric attenuation is 2 dB/km.

(f). To further explain the performance of the sensors, we obtain the eye patterns of sensor-2 at the output of the ELPF for different values of C_n^2 parameter as shown in Fig. 9. It is clear that as the C_n^2 parameter value increases, the eye diagram of the received signal deteriorates and becomes narrower.

It can be observed from the detailed performance analysis of the sensors that different ranges of the hybrid link can be obtained for different scenarios based on different combinations of the water bodies, atmospheric attenuation, and C_n^2 parameter of UWOC and FSO channels. For instance, maximum link range of 6.2 km (including SSMF length) can be achieved for water extinction coefficient, atmospheric attenuation, and C_n^2 parameter values of 0.043 m^{-1}, 2 dB/km, and 5×10^{-16} $m^{-2/3}$, respectively. Similarly, different ranges of the hybrid link can be estimated for different scenarios based on different combinations of the water bodies, atmospherics attenuation, and C_n^2 parameter of UWOC and FSO channels.

6. Conclusions

A single photo-detection, remodulate, and forwarding relay aided underwater wireless optical communication-single mode fiber-free space optics based hybrid link that supports underwater optical wireless sensor network has been proposed. Intensity modulation-direct detection scheme is used in this work to support the transmission of the data of eight sensors at a rate of 1 Gb/s. Wavelength translation from visible range to infrared has been performed using photo-detection, remodulate, and forwarding relay that is installed at remotely operated underwater vehicle. The performance of the sensors was analyzed for different water bodies and weather conditions of underwater and free space optical channels, respectively using metrics of Bit-error rate and Quality factor employing Gamma–Gamma channel model. Forward-error correction target BER of 10^{-4} for the sensors was achieved for different water bodies and weather conditions.

CRediT authorship contribution statement

Jawad Mirza: Writing – original draft, Supervision, Project administration, Methodology, Investigation, Formal analysis, Conceptualization. **Ahmad Atieh:** Writing – review & editing, Software, Methodology, Data curation. **Benish Kanwal:** Methodology. **Salman Ghafoor:** Conceptualization. **Ahmad Almogren:** Conceptualization. **Firdos Kanwal:** Writing – review & editing. **Imran Aziz:** Funding acquisition.

Declaration of competing interest

The authors declare that they have no known competing financial interests or personal relationships that could have appeared to influence the work reported in this paper.

Acknowledgment

This work was supported by King Saud University, Riyadh, Saudi Arabia, through Researchers Supporting Project number (RSP2024R184).

Data availability

Data will be made available on request.

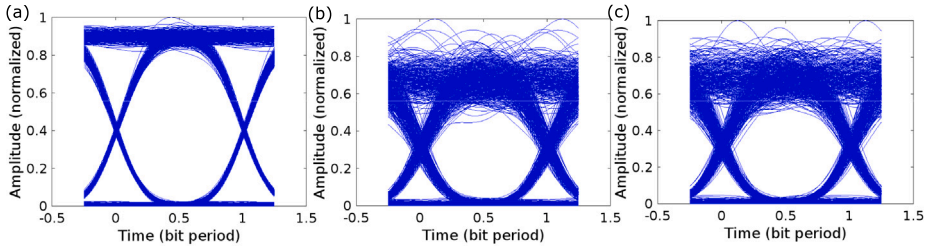

Fig. 9. Normalized eye patterns of sensor-2 for different values of C_n^2 parameter (a) 5×10^{-16} $m^{-2/3}$ (b) 5×10^{-14} $m^{-2/3}$, and (c) 5×10^{-12} $m^{-2/3}$. The value of atmospheric attenuation 2 dB/km.

References

[1] L. Nkenyereye, L. Nkenyereye, B. Ndibanje, Internet of underwater things: A survey on simulation tools and 5G-based underwater networks, Electronics 13 (3) (2024) 474.

[2] J. Mirza, F. Kanwal, U.A. Salaria, S. Ghafoor, I. Aziz, A. Atieh, A. Almogren, B. Kanwal, Underwater temperature and pressure monitoring for Deep-Sea SCUBA divers using optical techniques, Front. Phys. 12 (2024) 1417293.

[3] Z. Du, W. Ge, C. Cai, H. Wang, G. Song, J. Xiong, Y. Li, Z. Zhang, J. Xu, 90-M/660-Mbps underwater wireless optical communication enabled by interleaved single-carrier FDM scheme combined with sparse weight-initiated DNN equalizer, J. Lightwave Technol. 41 (16) (2023) 5310–5320.

[4] Z. Shen, H. Yin, L. Jing, X. Ji, Y. Liang, J. Wang, A power control-aided Q-learning-based routing protocol for optical-acoustic hybrid underwater sensor networks, IEEE Trans. Green Commun. Netw. 7 (4) (2023) 2117–2129.

[5] A.J. Aljohani, J. Mirza, S. Ghafoor, A novel regeneration technique for free space optical communication systems, IEEE Commun. Lett. 25 (1) (2020) 196–199.

[6] J. Mirza, S. Ghafoor, A. Hussain, All-optical generation and transmission of multiple ultrawideband signals over free space optical link, Opt. Eng., Bellingham 58 (5) (2019) 056103.

[7] L.B. Kumar, P. Krishnan, Multi-hop convergent FSO-UWOC system to establish a reliable communication link between the islands, Opt. Commun. 474 (2020) 126107.

[8] L-K. Chen, Y. Shao, Y. Di, Underwater and water-air optical wireless communication, J. Lightwave Technol. 40 (5) (2022) 1440–1452.

[9] W-S. Tsai, H-H. Lu, H-W. Wu, S-C. Tu, Y-C. Huang, S-E. Tsai, 500 Gb/s PAM4 FSO-UWOC convergent system with a r/g/b five-wavelength polarization-multiplexing scheme, IEEE Access 8 (2020) 16913–16921.

[10] S.R. Teli, C. G-Yanez, V.M. Icaza, R. P-Jimenez, Z. Ghassemlooy, S. Zvanovec, Hybrid optical wireless communication for versatile IoT applications: data rate improvement and analysis, IEEE Access 11 (2023) 55107–55116.

[11] S. Zhou, D. Ding, J. Wang, Y. Li, D. Yang, C. Bai, Performance analysis of hybrid FSO-UWOC dual-hop link for air-ocean communication, in: SPIE Eighth Symposium on Novel Photoelectronic Detection Technology and Applications, Vol. 12169, 2022, pp. 1079–1084.

[12] M.F. Ali, D.N.K. Jayakody, M.V. Ribeiro, A hybrid UVLC-RF and optical cooperative relay communication system, in: 10th IEEE International Conference on Information and Automation for Sustainability (ICIAfS), 2021, pp. 13–18.

[13] A.A. Sabri, S.M. Hameed, W.AH. Hadi, Last mile access-based FSO and VLC systems, Appl. Opt. 62 (31) (2023) 8402–8410.

[14] C-Y. Li, X-H. Huang, H-H. Lu, Y-C. Huang, Q-P. Huang, S-C. Tu, A WDM PAM4 FSO–UWOC integrated system with a channel capacity of 100 Gb/s, J. Lightwave Technol. 38 (7) (2019) 1766–1776.

[15] R. Deka, S. Anees, Performance analysis of HAPS integrated hybrid RF/FSO system cascaded with an UWOC link, in: 10th IEEE International Conference on Signal Processing and Integrated Networks, SPIN, 2023, pp. 750–755.

[16] J-Y. Wang, P. Feng, L-H. Hong, H-N. Yang, N. Liu, Performance evaluation and optimization of UAV-based hybrid Dual-Hop FSO/UOWC systems, IEEE Syst. J. 18 (2) (2024) 1020–1031.

[17] M. Singh, M.H. Aly, S.A. Abd El-Mottaleb, Performance analysis of a 448 Gbps PDM/WDM/16-QAM hybrid SMF/FSO system for last mile connectivity, Opt. Quantum Electron. 55 (3) (2023) 231.

[18] OptiSystem. https://optiwave.com/products/optisystem/.

[19] J. Mirza, A.J. Aljohani, M. Ijaz, S. Ghafoor, Combined transmission of PPM and WSK modulated optical signal over free space optical link enabling physical layer security, Optik 302 (2024) 171748.

[20] S. Arnon, D. Kedar, Non-line-of-sight underwater optical wireless communication network, J. Opt. Soc. Amer. A 26 (3) (2009) 530–539.

[21] J. Mirza, A. Atieh, M.I. Menhas, S. Ghafoor, M. Magam, L. Jamal, S.I. Mitu Sheikh, K.K. Qureshi, Design of an efficient Thulium-doped fiber amplifier for dual-hop earth to satellite optical wireless links, Ain Shams Eng. J. 14 (7) (2023) 101983.

[22] C. Qu, S. Ghafoor, A. Ahmad, J. Mirza, A.J. Aljohani, I. Aziz, A bidirectional free space optical link for last-mile terrestrial access links employing a novel wavelength shift keying technique, Opt. Quantum Electron. 56 (8) (2024) 1367.

[23] N.A.M. Nor, Z. Ghassemlooy, J. Bohata, P. Saxena, M. Komanec, M-A. Khalighi, Experimental investigation of all-optical relay-assisted 10 Gb/s FSO link over the atmospheric turbulence channel, J. Lightwave Technol. 35 (1) (2016) 45–53.

[24] J.G. Proakis, Digital Signal Processing: Principles, Algorithms, and Applications, Pearson Education India, 2001.

[25] C. Shen, Y. Guo, H.M. Oubei, T.K. Ng, G. Liu, K-H. Park, K-T. Ho, M.S. Alouini, B.S. Ooi, 20-Meter underwater wireless optical communication link with 1.5 Gbps data rate, Opt. Express 24 (22) (2016) 25502–25509.

[26] Lithium Niobate Modulators. https://www.thorlabs.com/newgrouppage9.cfm?objectgroup_id=3918.

[27] Erbium-doped Fiber Amplifiers. https://www.thorlabs.com/newgrouppage9.cfm?objectgroup_ID=10680.